Korean J. Chem. Eng., 19(1), 28-40 (2002)

Quality of CFD Models for Jet Flow Analysis for the Design of Burners and Boilers

F. Marias†, J. R. Puiggali*, M. Quintard and F. Pit*****

Laboratoire de Génie des Procédés de Pau, rue Jules Ferry, 64000 PAU - France
*Laboratoire Energétique et Phénomènes de Transfert, Esplanade des Arts et Métiers, 33405 Talence Cedex - France
**CNRS, Institut de Mécanique des Fluides de Toulouse, Allée du Prof. Soula, 31400 Toulouse - France
***Laboratoire de Génie des Procédés de Pau, rue Jules Ferry, 64000 PAU - France
(*Received 7 March 2001 • accepted 31 July 2001*)

Abstract–CFD models are increasingly used for the design and optimisation of boiler combustion chambers. Numerous commercial codes are available, and the user is confronted with making a proper choice for a particular application. In this paper, the accuracy and effectiveness of the popular code FLUENT™ is investigated in terms of the different turbulence models and numerical schemes that are bundled in the software. The tests are performed for different simple experiments, involving classical hydrodynamic conditions with no combustion. The conclusion of these tests involves also the additional criterion of the computational time required for achieving a reasonable accuracy.

Key words: Boiler, Simulation, Turbulence, Interpolation Scheme

INTRODUCTION

In order to use CFD codes under turbulent conditions, it is necessary to choose between the different proposed physical models [Leschziner and Rodi, 1981; Hogg and Leschziner, 1989a, b; Lien and Leschziner, 1994a, b; Elena and Schiestel, 1996; Bradshaw et al., 1996; Menter, 1996; Wilcox, 1994] and numerical algorithms [Leschziner and Rodi, 1981; Lien and Leschziner, 1994b; McKenty et al., 1999]. It is in general difficult to have a priori knowledge of the representativeness of these models, and the associated computational times are difficult to predict, thus making a choice a delicate matter.

For a given problem, the choice of the physical model, especially the turbulence model, requires knowledge of the physical parameters involved, and also indications about the required accuracy on some relevant quantities (average value at the outlet or at some location within the studied domain, instant values, ...). Once these choices are made, the feasibility and accuracy of the computations depend upon the choice of the numerical algorithm. In this paper, we present a study of the impact of the coupling between the different turbulence models and numerical algorithms that are available in the commercial CFD code Fluent™.

In order to evaluate the influence of these choices, three experimental situations that are commonly encountered in industrial boilers have been chosen as test cases. For these three cases, isothermal conditions, constant density, and no chemical reactions were assumed to ensure that turbulence was essentially controlled by the Reynolds number. These three cases are described below:

- A free, axisymetrical jet. For this particular configuration, experimental data were available [Modaress et al., 1982], as well as some numerical modelling [Wilcox, 1994; Berat, 1987].
- An axisymetrical jet confined in a cylindrical chamber and an annular jet, for which experimental data were also available [Habib and Whitelaw, 1983], as well as numerical results [Berat, 1987].
- The flow induced in a cylinder by a swirling device (swirler), for which experimental data were published by So and Mongia [1984], and numerical results were obtained by Hogg and Leschziner [1989b], and Ohtsuka [1995].

We will only consider here averaged fields, which are available in all the contributions cited above.

†To whom correspondence should be addressed.
E-mail: frederic.marias@univ-pau.fr

DESCRIPTION OF THE SIMULATION AND THE MODELS

Fluent™ offers the possibility to use the following turbulence models: a k-ε model, as proposed by Launder and Spalding [1972], an RNG k-ε model [Yakhot and Orszag, 1986], and the RSM model proposed by Launder et al. [1975]. At the same time, the user has to choose between three different numerical schemes, with different types of interpolation: Power Law interpolation, Second Higher Order Scheme, and Quick. Calculations were performed on a PC equipped with a 166 MHz Pentium processor.

1. The FLUENT Code

The code is popular, and we will only list here its principal features. This code uses a finite volume element technique [Patankar, 1980] to discretise the partial differential equations associated with the mass, momentum, and energy balance equations. The code allows simulating classical fluid mechanics and heating transfer problems, including chemical reactions. Interestingly, the code offers two major options. First, several turbulence models are programmed, and, secondly, the user may chose among various numerical schemes. The quality of the numerical prediction will essentially depend on the choice of these two essential features. Of course, additional choices must be made that may impact the quality of the simulations, for instance, the mesh size, the pressure/velocity algorithm,

or the grid orientation.

2. Interpolation Schemes

Fluent uses a Non-Staggered Control Volume Storage Scheme, which means that all discrete quantities are associated with the central node of the control volume. In the control volume approach, fluxes have to be determined at the volume boundaries using the node values. Fluent™ offers three different interpolation schemes [Fluent User's Guide, 1996]:

- Power law interpolation,
- Second Order-Upwind Interpolation,
-Quick Interpolation.

These schemes are not necessarily the best schemes available. Indeed, schemes that are more efficient have been proposed in the literature. However, they are not often implemented in commercial simulators. Since the purpose of our paper is restricted to the use of a particular code, namely FLUENT, we will use the three available numerical schemes to solve the Navier-Stokes equations. The reader can find further information about these schemes in appendix A.

3. Turbulence Models

In this paragraph, which is certainly not a treatise on turbulence, we remind the reader of the classical turbulence models in order to clarify what parameters must be introduced by the engineer. While turbulent flows have a very complex structure, involving 3D, unsteady vortices at different length-scales, it is often sufficient for engineering purposes to know the average pressure and velocity fields. Following Reynolds' ideas, one writes the instantaneous velocity as:

$$u_i = \overline{u_i} + u_i' \tag{1}$$

where $\overline{u_i}$ denotes the average velocity and u_i' the fluctuation.

With this nomenclature, the Reynolds stress tensor in the averaged Navier Stokes equations is written as

$$\tau_{ij} = -\rho\overline{u_i'u_j'} \tag{2}$$

This tensor is evaluated in the FLUENT code in three different manners, which are briefly outlined below.

Like for the numerical schemes, these choices do not entirely cover all turbulence models available in the literature. More up to date approaches are not usually implemented in commercial simulators.

3-1. First Order Models: k-ε and RNG k-ε Models

These two models use the classical concept of turbulent viscosity put forward by Boussinesq [1877]. The Reynolds stress tensor is evaluated by a classical linear expression involving the rate of strain tensor in which the sum of molecular and turbulent viscosity replaces the molecular viscosity.

The problem is of course the evaluation of the turbulent viscosity. It is determined through a correlation involving the turbulence kinetic energy, k, and its rate of dissipation, ε, which are defined by

$$k = \frac{1}{2}\overline{u_i'u_i'} \tag{3}$$

$$\varepsilon = \overline{\frac{\nu}{2}\left(\frac{\partial u_i'}{\partial x_j} + \frac{\partial u_j'}{\partial x_i}\right)^2} \tag{4}$$

The closure of the equations associated with these quantities is not discussed here. It requires three empirical constants, which are discussed in the literature [Launder and Spalding, 1972; Fluent User's Guide, 1996; Rodi, 1984]. An additional empirical constant, C_μ, links the turbulent viscosity, μ_t, to the velocity scale $k^{1/2}$, and to the length scale $k^{3/2}/\varepsilon$. This correlation is written as

$$\mu_t = \rho C_\mu \frac{k^2}{\varepsilon} \tag{5}$$

The basic idea of RNG method as applied to turbulence modelling is the elimination of small scale eddies through modifications in effective viscosity, force and linear coupling [Yakhot and Orszag, 1986]. Within this framework, new equations are obtained for the turbulence kinetic energy, k, and its rate of dissipation, ε, and a new correlation is proposed for the turbulent viscosity, namely

$$\mu_t = \mu\left[\left(1 + \sqrt{\frac{C_\mu}{\mu}}\frac{k}{\sqrt{\varepsilon}}\right)^2 - 1\right] \tag{6}$$

The constant C_μ is evaluated theoretically and depends on the flow rotation rate, and constants that appear in the transport equations for k and ε were obtained theoretically [Yakhot and Orszag, 1986; Fluent User's Guide, 1996].

3-2. Second Order Model: RSM

Contrary to the first order models, which are based on a model for the Reynolds stress tensor, the RSM Model (Reynolds Stress Model) evaluates the stress tensor components at every point by solving the associated transport equations. These equations contain higher order terms $\rho\overline{u_i'u_j'u_k'}$ as well as pressure/velocity coupling terms that must be determined.

The final model requires nine constants that must be evaluated empirically [Launder et al., 1975; Launder, 1989].

4. Boundary Conditions

In order to carry out the computational effort, specific numerical treatment is required at each area bounding the computational domain.

4-1. Inlet Areas

The boundary conditions in the different simulations were based on experimental data, i.e., velocity profiles, kinetic energy and dissipation. These values were assigned to the nodes of the control volumes closer to the physical boundary.

4-2. Outlet Areas

At the outlet, we assume that we have a fully developed flow, which is translated numerically by imposing zero normal gradients.

4-3. Walls

The presence of walls requires a specific treatment [Wilcox, 1994; Launder, 1989; Launder and Spalding, 1974]. The three-zone structure of the turbulent boundary layer is described through two alternate models [Wilcox, 1994; Patankar, 1980; Launder and Spalding, 1974].

An accurate method would require the calculation of the turbulent and average quantities within the boundary layer itself. This would impose the choice of very fine grids close to the walls, thus leading to heavy calculations. The alternate route is to use a wall turbulence model, which links empirically the stress tensor to the velocity close to the wall. The approach that has been adopted in this paper consists in putting the first node in the logarithmic zone of the boundary layer, and then using wall functions. See appendix B for more details about these functions.

COMPARISON BETWEEN SIMULATIONS AND EXPERIMENTS: METHODOLOGY

Test cases are presented in the next section in order to evaluate the influence of the turbulence models and the numerical schemes. In this section we discuss the methodology for doing such comparisons. CFD codes give a great deal of information, in particular, local velocity and pressure fields are available. Therefore, the first idea would be to define comparison criteria on the basis of these fields. Mathematical norms, for instance, could be introduced for this purpose, and one possible choice is discussed below.

1. Definition of Average Error

In the definition of the comparison criterion, we took into account the following two difficulties: (i) velocity profiles are the most common data available, (ii) the number of experimental points, N, is limited. We adopted the following averaged error

$$E = \frac{1}{N}\sum \frac{|\phi_{exp} - \phi_{num}|}{|\phi_{exp}|} \quad (7)$$

as an indication of the quality of the simulations, where ϕ represents in general some velocity data.

However, the application of such criteria requires that enough data are available, which is not often the case for the engineer. On the contrary, pressure and velocities may be available at some definite locations, most often at the boundaries of the simulated domain. Error criteria can be built on this limited information, which of course cannot be considered as good approximation for the norm associated with the entire domain. It must be emphasised that the best numerical choice in terms of these limited criteria could prevent the use of a code that would give more valuable information as a whole. We choose to define errors associated with this limited scope in a manner similar to the definition proposed in Eq. (7).

Some visual information may also be available (streamlines visualisation), that could be used for comparison. Since distributed data are available from the numerical results, it is not difficult to perform a semi-quantitative comparison between the observed fields and the computed ones. In the three test cases presented in Sec. 4, such information was not available, and we shall not discuss this point further.

Of course, computational requirements, memory and CPU time, are important criteria that must be known to engineers. Indications will be presented at the end of Sec. 4 in the synthesis of the tests cases.

Other criteria may involve very important problems such as:

1. definition of the boundary conditions, especially at the inlet of the domain,
2. information required to run the model, which may not be readily available,
3. meshing of the studied domain.

TEST CASES

Three cases have been selected from literature, which cover the most relevant configurations in burner systems:

- free jet,
- confined co-axial jets,
- swirling annular jet

In order to minimize the influence of the grid size, the optimum mesh size has been determined for each configuration by performing simulation with the k-e model and power law interpolation. The number of nodes has been increased until convergence.

1. Case 1: Free Jet

The reference experimental data are those obtained by Modaress et al. [1982], when their primary jet is free of solids, using laser anemometry. These results were chosen partly because experimental conditions were given in a detailed manner so it was possible to carry out a numerical simulation.

1-1. Experimental Conditions

The experimental configuration is presented in Fig. 1. Air at a temperature of 300 K is introduced through an injector. The injector diameter is d and its length is long enough so a developed flow is obtained. The jet spreads within a cylinder, diameter D, to avoid surrounding perturbations. In order to perfectly set the boundary conditions, the authors introduce a low velocity secondary stream. This configuration is representative of a classical injection within a combustion chamber. The geometrical characteristics as well as the flow characteristics measured at x=0.1d are given in Table 1.

Values of the axial velocity have been measured along the axis, as well as its radial evolution at x/d=20 (x=0.4 m), within the self-similarity zone.

1-2. Numerical Parameters

The studied domain corresponds to an angular sector of 1 radian

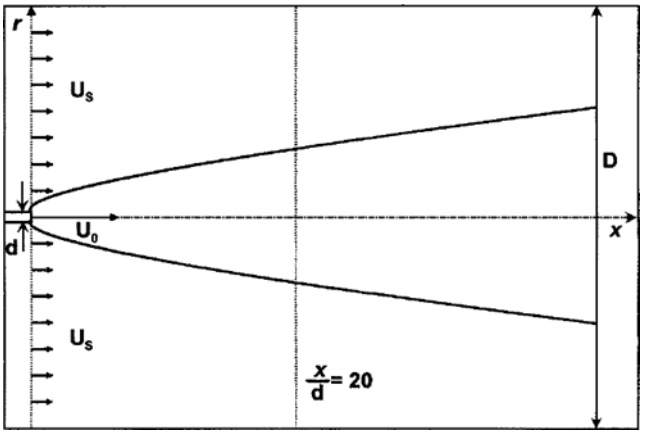

Fig. 1. Characteristics for the experiment of Modaress et al. [1982].

Table 1. Characteristics of Case 1 [Modaress et al., 1982]

Injector diameter	d=0.02 m
Diameter of the combustion chamber	D=30d
Velocity on the axis	U_0=13.4 m/s
Profile of primary velocity	$\frac{U(r)}{U_0} = \left(1 - 2\frac{r}{d}\right)^{1.66}$
Intensity of primary turbulence	$\frac{u'}{U_0} = 0.04 + 0.1\frac{r}{d}$
Secondary velocity	U_s=0.05 m/s
Secondary intensity of turbulence	$\frac{u'_s}{U_s} = 0.1$

with axial limits situated at x=0.1d and x=1 m. The 2D grid is axis-symmetrical, with 200 · 20 nodes. The axial direction corresponds to half the chamber (D/2) with 20 nodes, 4 nodes corresponding to half the tube (d/2). The grid has a variable mesh size along both directions.

The boundary conditions used to simulate the jet consist in imposing the profiles of the velocity, turbulence kinetic energy and dissipation. The first two quantities are taken from experimental data as explained in Table 1. For the entrance dissipation values, we used a length-scale, l, deduced from the mixing length, l_m, as introduced by Leschziner and Rodi [1981]. This choice is based on the fact that this turbulence model, initially proposed by Prandtl, is efficient when modelling flow in pipes [Wilcox, 1994]. We have

$$\varepsilon = C_\mu \frac{k^{3/2}}{l} \qquad l = 0.55 l_m \tag{8}$$

$$\frac{2l_m}{d} = 0.14 - 0.08\left(1 - \frac{2y}{d}\right)^2 - 0.06\left(1 - \frac{2y}{d}\right)^4 \tag{9}$$

For modelling the secondary flow at the inlet, the velocity, turbulence kinetic energy and dissipation are taken as constants. These constants are evaluated by assuming that the injector, because of its small dimension, has no influence on the behaviour on the secondary flow.

1-3. Analytical Model

In this evaluation, we found it interesting to compare also with the theoretical results obtained by Craya and Curtet as referenced by Monnot [1978]. Their free jet theory in infinite atmosphere assumes that the fluid follows Euler's equations outside of the jet, and that the reduced velocity profile is independent of x in the self similarity region, i.e.,

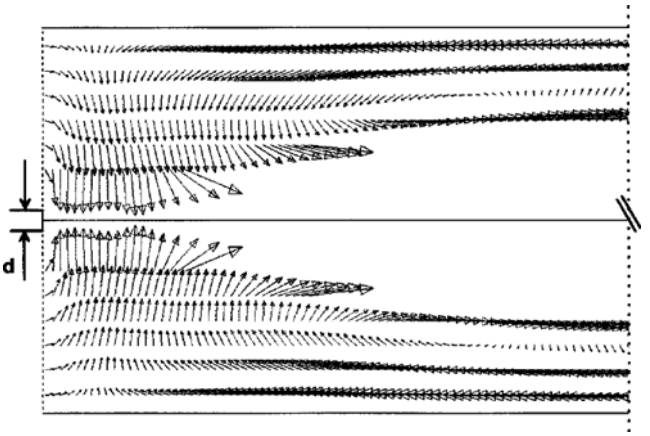

Fig. 2. Example of velocity vectors obtained by simulation of Free Jet. Couple Model/Scheme k-ε/PowerLaw. Maximal represented scale : 0.4 m/s.

$$U(r,x)/U_{axe}(x) = f(r/d) \tag{10}$$

1-4. Comparison with Experimental Data

The velocity field obtained from the numerical simulations is presented in Fig. 2. The comparison between these results and the experimental and theoretical values is presented in Fig. 3.

1-5. Discussion

From the results in Fig. 2, we distinguish two important phenomena. The primary flow is driven by the secondary flow immediately at the entrance, and because of the small mass flow-rate carried by the secondary stream, recirculation occurs to achieve turbulence friction. One would require that both the mass flow-rate of the recirculated flow and the location of the vortex be accurately pre-

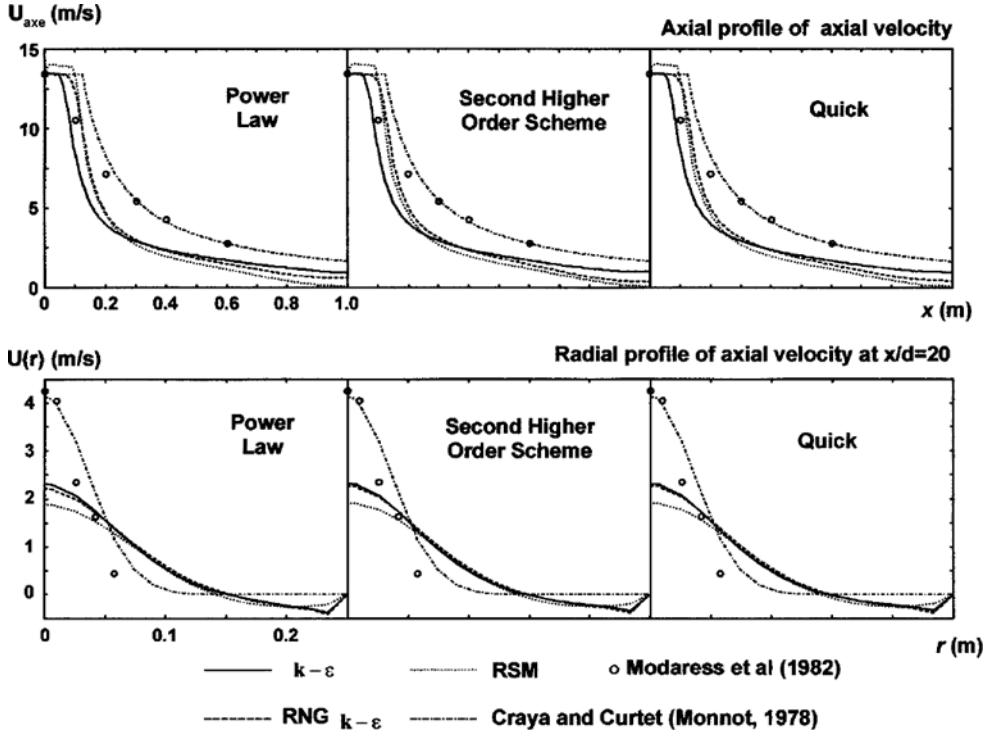

Fig. 3. Axial and radial profile of axial velocity (Free Jet).

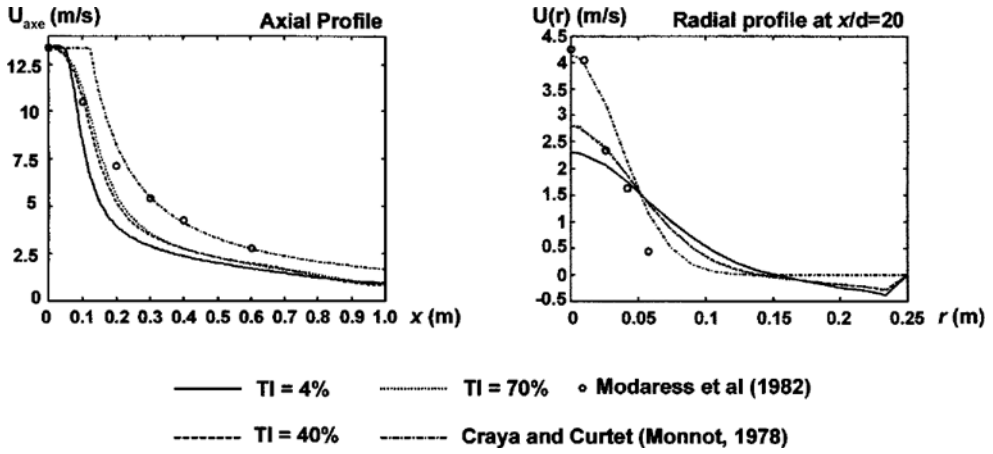

Fig. 4. Axial and radial profile of axial velocity evolution as a function of turbulence intensity in the Free Jet case (Model k-ε, Scheme Power Law).

dicted. These specific data are not available.

Following the methodology developed in paragraph 3, the experimental profiles are compared to the results of the numerical simulations, for the different turbulence models, and for a fixed interpolation scheme. The results are shown on Fig. 3. They show that the numerical results are qualitatively correct. The axial evolution of the axial velocity features a zone where the flow can be considered as laminar. Then, the velocity decreases because of the turbulent diffusion and dissipation. Furthermore, the Gaussian profile in the self-similarity region is correctly represented.

However, the examination of specific points, even if no experimental data are available, shows that the predictions are not accurate. For example, the numerical models give different predictions for the length of the potential region or the thickness of the jet.

• *Conclusion relative to the interpolation scheme*: increasing the number of points involved in the interpolation scheme does not furnish any improvement in the behaviour of turbulence models. Indeed, they do not exhibit any significant differences and no specific distinction will be made in the following analysis.

• *Conclusions to be shared by the three turbulence models*: neither of the turbulence models correctly represents the quantitative evolution of the axial velocity. This conclusion can be drawn for both the axial and the radial profile of axial velocity. This is due to the relative overestimation of radial diffusion of momentum over axial one. For instance, there is a factor 2 difference between numerical simulations at x=0.4 m on the axis and for the first order models, and a factor 2.5 for the RSM model at the same location.

• *Conclusions to be shared by the first order models:* some workers [Berat, 1987; Launder and Spalding, 1974] have compensated the radial momentum diffusion overestimation decreasing the turbulence viscosity through a correlation between C_μ and the width of the mixing zone, and also by decreasing the dissipation rate using a similar idea. In the re-circulating zone due to the confinement, the jumps observed at the node closest to the wall are due to the use of wall models; indeed, the positive value of wall shear stress obtained from turbulence kinetic energy, necessarily positive, is inadequate at this location [Wilcox 1994].

• *Conclusion relative to the k-ε model*: this model is the best in the estimation of the far longitudinal profile of axial velocity. This allows this model to be the best predictor of the radial velocity profile of axial velocity in the self-similarity region. Increasing turbulence intensity (defined as the ratio of the root mean square turbulent velocity fluctuations to the mean flow velocity) at the inlet, and calculating the dissipation by using Eq. (8) and (9) leads to better simulation results for the k-ε model, as shown on Fig. 4. This emphasises that the k-ε model is more efficient at large Reynolds number.

• *Conclusion relative to the RNG k-ε model:* although no experimental data available, this model seems to be the best for the prediction of the potential region because always closest from the experimental value located at x=0.1 m.

• *Conclusion relative to the RSM model*: it overestimates the maximum velocity of about 5% in the potential region, which is of physical nonsense. Furthermore, this model is the worst in the prediction of the longitudinal dependence of the axial velocity. That is why we advise users to take extreme care in using this model, within the free jet case and the Fluent™ environment.

The best prediction for this particular configuration remains the analytical model by Craya and Curtet (quoted by Monnot in 1978). This one exhibits major improvements in the radial and axial diffusion of momentum.

2. Case 2: A Re-Circulating Flow Composed of Two Confined Co-Axial Jets with Expansion

This more complex experiment is destined to the study of turbulence triggered by two isothermal, confined, co-axial jets. The detailed experimental results of Habib and Whittelaw [1983] have been selected for our numerical computations.

2-1. Experimental Conditions

The experimental configuration is presented in Fig. 5. The two jets are supplied with air at 283 K. The ratio between the maximal velocity in the annulus and the maximal velocity in the primary flow is equal to 3. The Reynolds numbers ($Re_a=U_a d_h/\nu$, $Re=U_0 d/\nu$) that are calculated with these maximum velocities are equal to 77500 and 18500, respectively. The upstream pipe lengths are such that the fully developed velocity profiles are well established. The geometrical characteristics as well as the flow characteristics are given

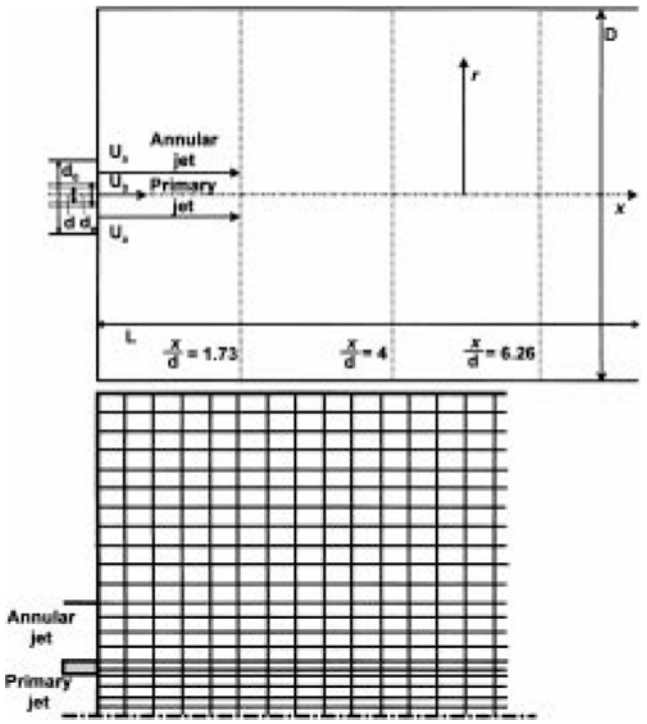

Fig. 5. Characteristics of Habib and Whitelaw experiment [1983]. Zoom on the grid near the inlets.

in Table 2.

Following the methodology developed in the previous case, the boundary conditions are extracted from experimental data. We used

Table 2. Geometrical characteristics for the experiment of Habib et Whitelaw [1983]

Interne diameter (primary flow)	d=0.0161 m
External diameter (primary flow)	d_e=0.0216 m
Annulus diameter	d_0=0.0445 m
Diameter	D=0.125 m
Chamber length	L=0.595 m

the values obtained by Durao and Whitelaw [1973] for the average axial velocity, the Reynolds stress tensor, and the dissipation in the primary flow. The required values for the flow in the annulus were those published by Brighton and Jones [1964]. These profiles are presented in Fig. 6.

Experimental values for the axial velocity are available for the axis, as well as radial profiles at x/d_0=1.73; x/d_0=4 and x/d_0=6.26.

2-2. Numerical Parameters

The studied domain corresponds to an angular sector of 1 radian with axial limits situated at the outlet of the injectors and x=1 m. The 2D grid is axis-symmetrical, with 200 · 20 nodes. The axial direction corresponds to half the chamber (D/2) with 19 nodes, 5 nodes corresponding to half the primary injector (d/2), 3 nodes for its thickness and 5 nodes are used for half the annulus. A zoom representing the grid near the inlets is sketched on Fig. 5.

The boundary conditions correspond to given axial velocity profiles and turbulence kinetic energy profiles for the k-ϵ and RNG k-ε models, and Reynolds stress tensor profiles for the RSM model. The values used are the experimental data presented in Fig. 6. The turbulence kinetic energy is calculated from the normal component of the Reynolds stress tensor for the first order model.

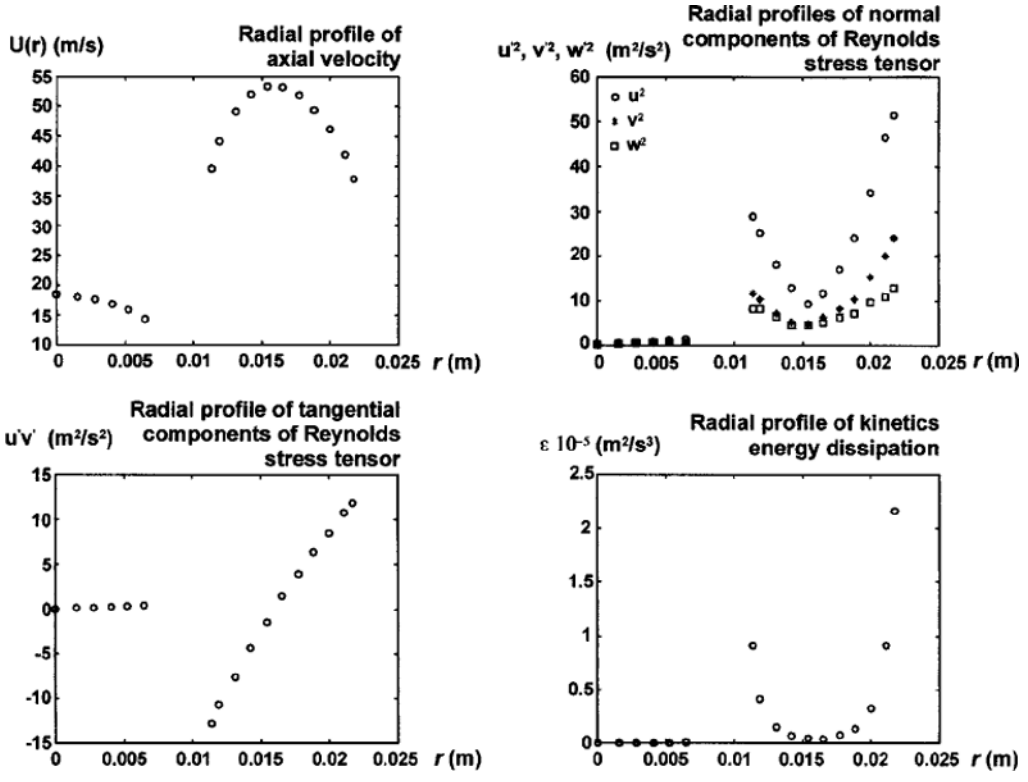

Fig. 6. Boundary conditions used for the simulation of the experiment of Habib and Whitelaw [1983].

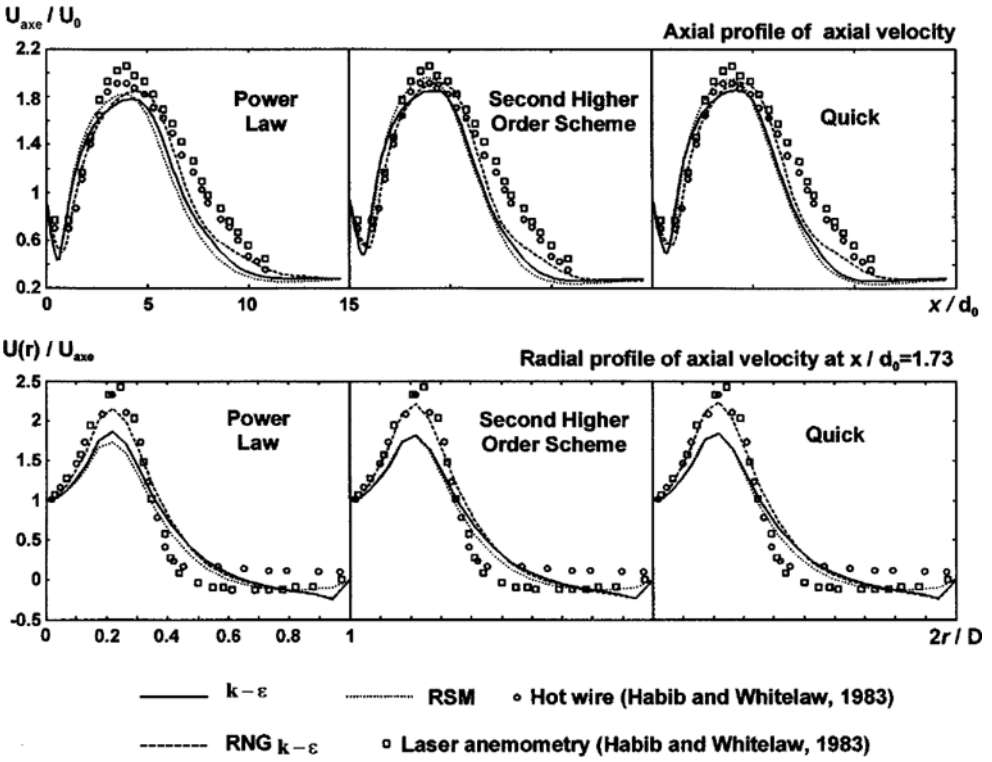

Fig. 7. Axial and radial profiles of axial velocity (Confined Jet).

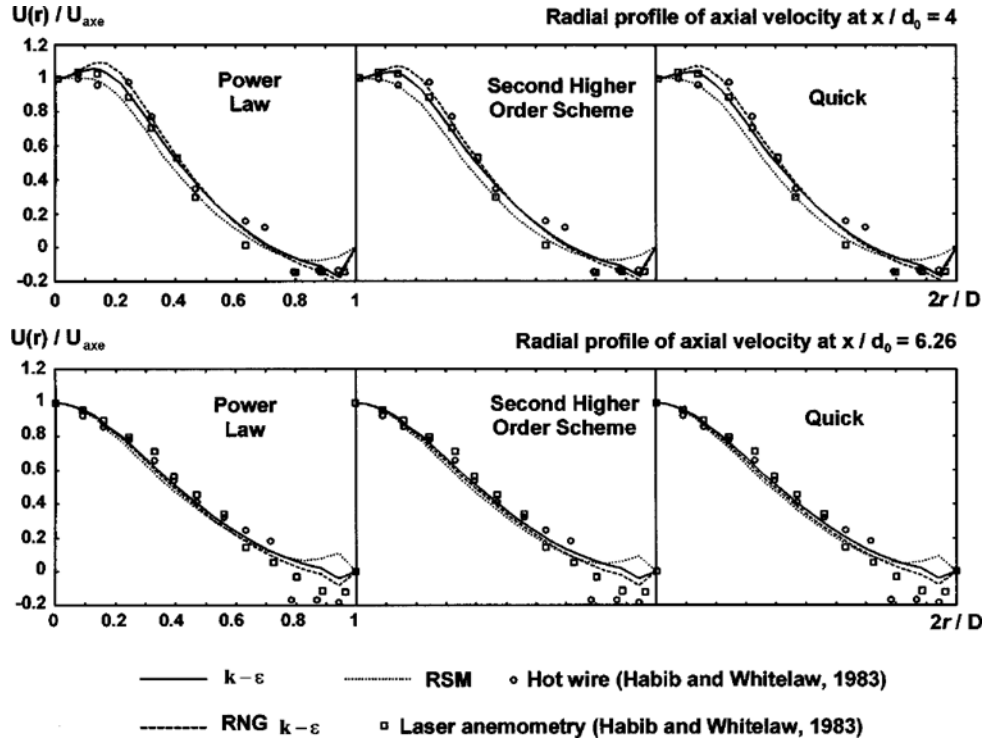

Fig. 8. Radial profiles of axial velocity (Confined Jet).

2-3. Comparison with Experimental Data

Experimental data and numerical results are compared on Figs. 7 and 8. The experimental data were obtained by using two different techniques: laser or hot wire anemometry. Even if these techniques are rather different, they provide similar results outside re-circulating zones (Figs. 7 and 8).

2-4. Discussion

Qualitatively and for the nine model/algorithm couples, the axial

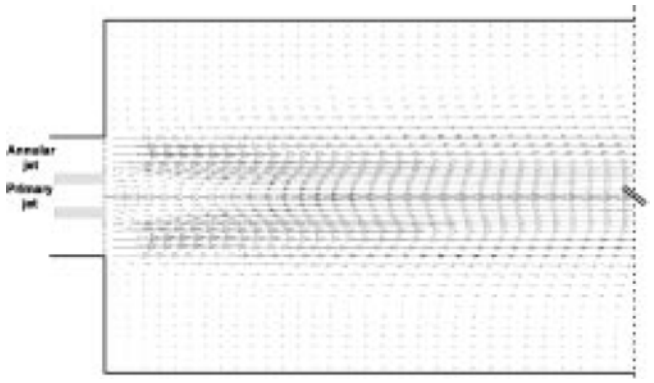

Fig. 9. Example of velocity vectors obtained by simulation of Confined Jet Couple Model/Scheme: RSM/Power Law. Maximal represented scale: 53 m/s.

evolution of the axial average velocity presented in Fig. 7 shows a good agreement between experiments and computations. Indeed, several features like (i) the decrease of axial velocity by diffusion from the primary to the secondary flow for $x/d_0 < 1.8$ (Fig. 9), (ii) its increase to a maximum after mixing of the two jets, then (iii) its rapid decreasing, are well represented. In addition, the radial profiles of the axial component of the average velocity within the mixing zone (Fig. 7) and upstream (Fig. 8) are similar to the experimental profiles.

• *Conclusion relative to the interpolation scheme*: in the case of the confined co-axial jets, some differences arise shifting from one algorithm to another. More precisely, the location of the axis minimum velocity as well as the amplitude and position of the maximum velocity are affected by the choice of the scheme (Fig. 7). This is particularly true in the case of the RSM model on the axis, and in the case of the RNG k-ε model for the radial profile of axial velocity in the mixing zone (Fig. 7, $x/d_0 = 1.73$). However, far downstream (Fig. 8), there are no significant differences in the use of these algorithms.

• *Conclusions to be shared by the three turbulence models:* as in the case of free jets, axial diffusion of momentum is underestimated in the mixing zone. This is illustrated in Fig. 7 where one can see that all models underestimate the value of the axial velocity during its decrease and overestimate the width of the maximum velocity peak. It is difficult to discuss the problem of recirculating flows near the walls since laser and hot wire anemometry do not give similar answers at these locations. Hot wire anemometry does not allow distinguishing recirculating flows, while laser anemometry does provide such information. The predictions given by the different numerical models are within the range of data provided by both experimental techniques, save in the neighbourhood of the walls. Indeed, the use of wall functions in the numerical models leads to jumps that are not physical.

• *Conclusions to be shared by the first order models:* both the k-ε and the RNG k-ε show limitations in the estimation of the maximum axial velocity along the axis. Moreover, used with wall functions, the model leads to unphysical jumps near the wall (Figs. 7 and 8).

• *Conclusion relative to the k-ε model*: within this case study, this model seems to be the worst. Indeed, both axial and radial profiles (mixing zone, Fig. 7) exhibit some limitations in the estimation of amplitude and position of extremum points. Thus, we advise against its use in such a configuration.

• *Conclusion relative to the RNG k-ε model:* except apart from the axis maximum velocity location prediction, this model is the best suitable for this configuration. It always gives the best result for the radial profiles and for the longitudinal decrease of axial velocity.

• *Conclusion relative to the RSM model*: this model may be used for the prediction of the maximum axial velocity on the axis, once coupled with a high order interpolation scheme. However, far downstream after the injectors, (Fig. 8, $x/d_0 = 6.26$), the RSM model does not predict any recirculating flow. This may lead to a bad estimation of the attachment point in the combustion chamber and, in hot simulations, in bad heat transfer computations at this point.

3. Case 3: Swirling Flow (Swirler)

This experiment is aimed at determining the flow characteristics after a swirling device. Such devices are essentially used in diffusion flame burners. The fluid affected by the swirl is the combustive, while the fuel is injected at the centre of the system. For the simulation, experimental results obtained by So et al. [1984] were used. We emphasise the fact that these flows are much more complicated than the flow encountered in the previous cases. This configuration has already been numerically simulated by Ohtsuka [1995], and Hogg and Leschziner [1989]. However, a comparison with these results is delicate since their numerical domain starts after the swirling device.

3-1. Experimental Conditions

Fig. 10 shows a sketch of the experiment. Air is brought to the swirler through a pipe with a diameter equal to D=120 mm at a temperature equal to 293 K. The flow is axis-symmetric. Turbulence is well developed since the Reynolds number is $5.49 \cdot 10^4$, which corresponds to an average velocity of 6.8 m/s.

The swirler is built of 15 blades (angle 66°) that do not touch the pipe axis. On this axis there is a circular obstacle of 53 mm, which plays the role of a flame stabilising device like in industrial burners. The swirl number obtained at the outlet is equal to 2.25 [So et al., 1984]. This number is calculated from the following formula:

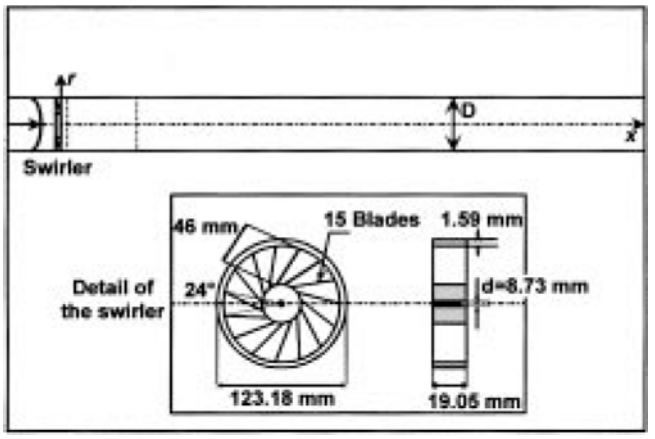

Fig. 10. Characteristics for the experiment of So and Mongia [1984].

$$S = \frac{\iint r W \vec{V} d\vec{A}}{\bar{r} \iint_A U \vec{V} d\vec{A}} \quad (11)$$

The central gas injector (closed in the case here) has a diameter equal to d=8.73 mm.

The experimental data at our disposal are the radial profile of the axial and circumferential components of the average velocity at x/d=1; x/d=5; x/d=10.

3-2. Numerical Parameters

The grid is a 3D grid with 11*29*72 nodes in the I, J, K directions. The axial limits of the domain are located at 3 cm upstream of the device, and 40 cm downstream. This grid represents a 15° of the entire geometry. In order to decrease the computational requirements, we have used the symmetry of the system (Fig. 11). The boundary conditions are limited to the airflow conditions in the pipe. Conditions like in the free jet case have been chosen, i.e., velocity profile, turbulence kinetic energy, and dissipation. The normal components of the Reynolds stress tensor are given the initial value 2/3k when using the RSM model (isotropic turbulence).

3-3. Comparison with Experimental Data

Numerical predictions are compared to the experimental data in

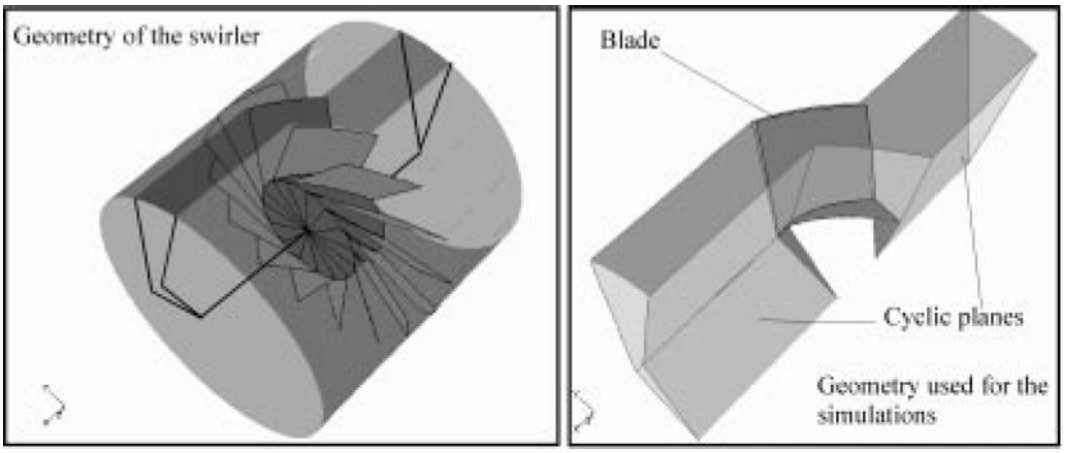

Fig. 11. Geometry of revolution and geometry used for computations.

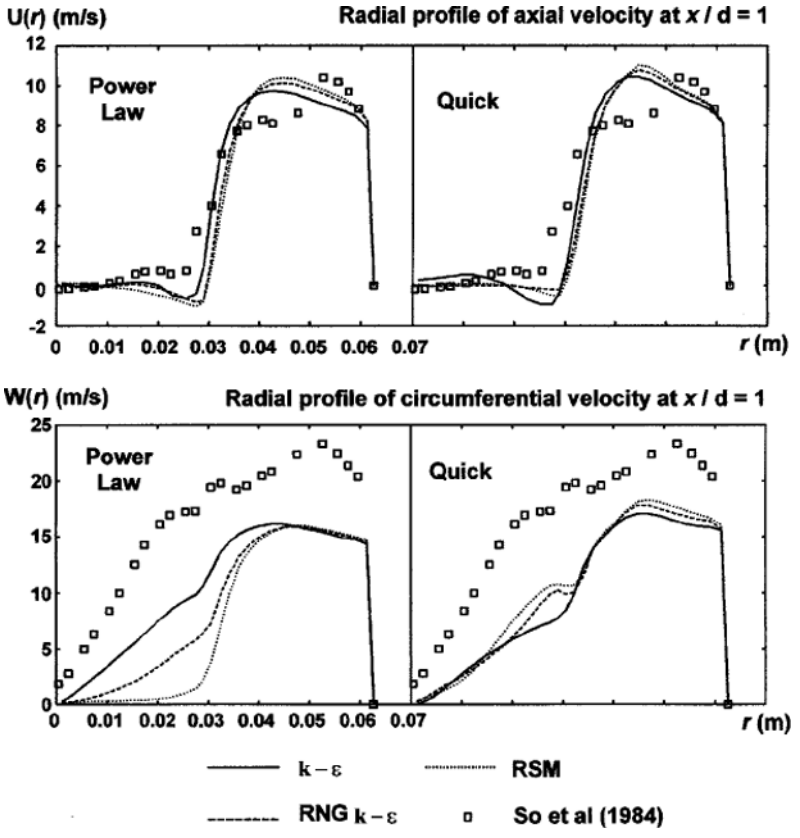

Fig. 12. Radial profiles of axial and circumferential velocity (Swirler).

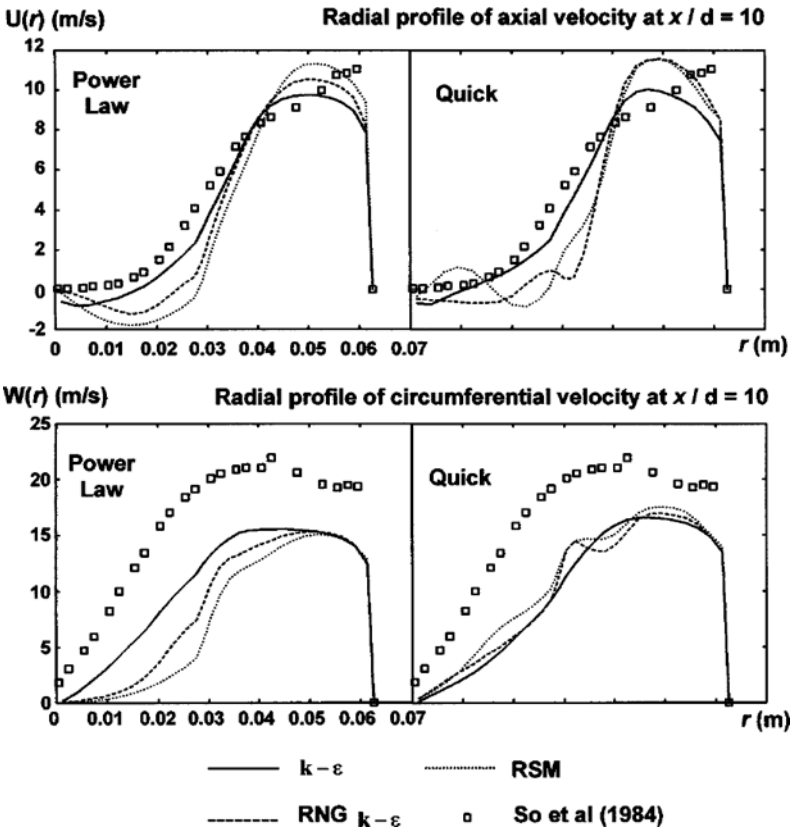

Fig. 13. Radial profiles of axial and circumferential velocity (Swirler).

Figs. 12 and 13. Because of failed convergence, the results with the Second Higher Order Scheme are not given. This may prevent the use of this algorithm when solving for flows with high tangential strain.

3-4. Discussion

Qualitatively, all flow features near or far from the device are correctly captured by the numerical simulations (Figs. 12 and 13). The forcing of the airflow near the wall by the stabilising disk is well represented (radial profile of the axial velocity). It is the same for the solid behaviour in the centre of the cylinder and free vortex behaviour near the wall (radial profile of the circumferential velocity).

• *Conclusion relative to the interpolation scheme*: whereas the k-ε turbulence model is almost independent of the interpolation scheme, more sophisticated models are more affected by the use of the quick scheme. More precisely, near the swirler (Fig. 12), the RNG k-ε and RSM models give better predictions using such an algorithm. Quantitatively, a most interesting effect to be studied is the recirculation induced by the stabilising disk. This effect is very important when estimating the stability of flames. For instance, when considering the radial evolution of the axial velocity close to the swirler, the six numerical simulations indicate that the fluid recirculates at the radius corresponding to longitudinal projection of the disk boundary (r=0.026 m). The flow-rate participating to this recirculation is more important for the most developed models (RNG, RSM) in the case of the Power Law scheme. This is the inverse behaviour with the Quick scheme. Moreover, the use of such a scheme leads to a better estimation of the axial velocity near the wall and near the swirler (Fig. 12), and to a better representation of the solid body behaviour near the swirler when RNG k-ε and RSM models are used. Nevertheless, because of the numerical instabilities arising, conclusions are drastically different far downstream from the swirler (Fig. 13).

• *Conclusions to be shared by the three turbulence models*: due to the complexity of the physical phenomena associated with the swirl, the qualitative prediction of the swirl is not always realistic. For instance, the decrease in axial velocity as a function of the radius, far from the device (Fig. 13), as predicted by all the models, is in contradiction with experimental results. Moreover, we are forced to observe that far from the swirling device, none of the models gives realistic simulations of the behaviour near the cylinder centre. The recirculating flows produced by the simulations are physically unrealistic. As previously indicated, the profiles of the orthoradial velocity are qualitatively well reproduced. This is not true from a quantitative point of view. None of the six tested couples allows a correct evaluation of the slope and maximum value of the tangential velocity near or far from the device (Figs. 12 and 13).

• *Conclusions to be shared by the first order models:* in this configuration, where the swirl effect is dominant, there is not any conclusion to be shared by the RNG k-ε models.

• *Conclusion relative to the k-ε model*: as previously quoted, increasing the level of interpolation does not significantly modify the behaviour of this model. However, regarding the radial profile of orthoradial velocity, it should be noted that the k-ε model should be coupled with the power law scheme in swirl dominant flow.

• *Conclusion relative to the RNG k-ε model:* although this model

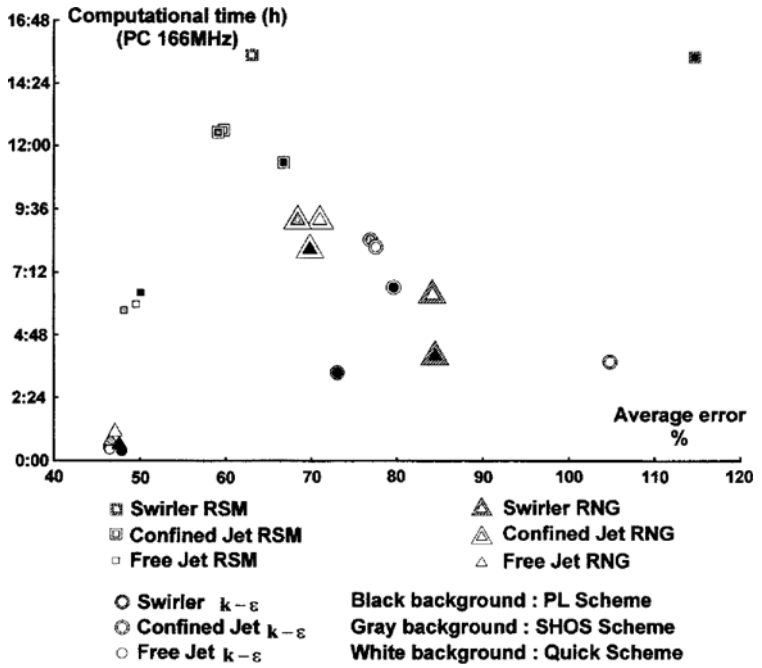

Fig. 14. Average error and computational time.

is expected to give the more precise information in swirl dominated flow, there is no point, in this particular configuration, where it increases the relevance of the numerical estimation.

• *Conclusion relative to the RSM model*: coupled with the power law scheme, this turbulence model is the only one able to represent the amplitude of the maximum of axial velocity (Figs. 12 and 13). Nevertheless, because of the bad prediction for the orthoradial velocity and of the numerical instabilities arising when used with an improved algorithm, this advice is not to use this model in such a configuration.

4. Analysis in Terms of Computational Time and Average Error

Fig. 14 shows the results obtained with the different simulations in terms of computational time and average error.

In the case of the free jet, Fig. 14 does not bring additional information since the retained average error goes from 46 to 50.5% depending on the configurations. On the opposite, this figure shows an interesting result about the computational time required for a good convergence. With this criterion in mind, it seems that the use of RSM model is not interesting if the knowledge of the Reynolds tensor at each grid point is not required.

The points relative to the confined flow have been calculated from the experimental data obtained by laser anemometry, in order to be compatible with other experiments. In this configuration, Fig. 14 shows that the choice between the different models is trivial. As expected, the accuracy increases when increasing the complexity of the turbulence model or when taking more accurate numerical schemes. Of course, the computational time increases accordingly, and accuracy must be balanced against the use of large computer resources.

In the case of the swirler, the accuracy cannot be retained as a quantitative criterion. The average error, on the contrary, seems to be more selective since the values obtained for the different numerical couples are between 62 and 115% (Fig. 14). From this figure, it may be concluded that the accuracy of the predictions is improved when more accurate numerical schemes are used with the more elaborated turbulence models. However, a simple numerical scheme is efficient with the k-ε model. Finally, it must be emphasised that the criterion to be retained for the choice between the RSM/Quick model and the k-ε/Power Law model is the computational time. For a similar accuracy, the computational time for the RSM/Quick model is five times the computational time for the k-ε/Power Law model. Once again, it seems that second order models are not practical, especially if the knowledge of the Reynolds stress tensor at each grid point is not required.

CONCLUSION

1. The study of the different numerical results and tests cases allows us to conclude that all models give realistic behaviours, at least qualitatively.

2. Quantitatively, and for a given configuration, the choice of the model/scheme pair depends on the particular point that is taken for the analysis. None of the models provide acceptable results for *all the criteria* that have been defined and tested.

3. The use of an average error is not practical for the engineer, since it does not put the emphasis on specific flow properties. However, it gives a valuable criterion for comparing experimental data and numerical predictions for complex flows.

4. For the tested configurations, the choice of the interpolation scheme has not affected significantly the final results. The most stable scheme, i.e., the power law scheme, must be used preferentially.

5. Computational times depend highly on the choice of the model/scheme pair. While the CPU time was less than 16 hours for all tested configurations, which is not very long, the user would expect major difficulty when using these tools for a real boiler with a

million nodes. In that case, the computational time would become the major issue, which would certainly preclude the use of the RSM model. However, one should remember that this model is the only one providing the Reynolds stress tensor values. In terms of the interpolation scheme, the power-law scheme leads in general to smaller computational times.

6. None of the models available in FLUENT have a universal applicability. There is no a priori indication that would tell the user what choice should be made. We believe that the engineer should run the different turbulence models on a particular case, and extract all relevant information from the obtained simulations. Of course, this conclusion is general and can be applied to all CFD packages available, since they use the same turbulence-models.

APPENDIX A: DISCRETIZATION PROCEDURES

The power law interpolation scheme in Fluent computes the face value of a variable, ϕ, using the exact solution to a one-dimensional convection-diffusion equation, where the different parameters of the equations are assumed to be constant over the studied cell. The result of such an equation is:

$$\frac{\phi(x)-\phi_0}{\phi_L-\phi_0}=\frac{\exp\left(Pe\frac{x}{L}\right)-1}{\exp(Pe)} \qquad Pe=\rho\frac{uL}{\Gamma}$$

In this last equation, ϕ_0 and ϕ_L represent the value of ϕ at the centre of two adjacent cells, and $\phi(x)$ stands for the required face value. Thus the face value depends upon the value of the Peclet number. Indeed, if its value is far greater than 1, the value of ϕ at x/2 is equal to its upstream value, and the power law scheme is nothing else than a first-order upwind scheme.

In the case of the Second Order Upwind Interpolation and the face value is computed by using the value of the two upstream cell centre (ϕ_0 and ϕ_{-1}):

$$\phi(x)=\left[\frac{\Delta x_{-1}+2\Delta x_0}{\Delta x_{-1}+\Delta x_0}\phi_0-\frac{\Delta x_0}{\Delta x_{-1}+\Delta x_0}\phi_{-1}\right]$$

In this last equation, Δx_{-1} and Δx_0 represent the characteristic size of the two upstream cells.

Finally, the Quick Scheme uses the two upstream cell values and the downstream cell value to compute the desired face value:

$$\phi(x)=\frac{3}{4}\left[\frac{\Delta x_L}{\Delta x_0+\Delta x_L}\phi_0+\frac{\Delta x_0}{\Delta x_0+\Delta x_L}\phi_L\right]+\frac{1}{4}\left[\frac{\Delta x_{-1}+2\Delta x_0}{\Delta x_{-1}+\Delta x_0}\phi_0-\frac{\Delta x_0}{\Delta x_{-1}+\Delta x_0}\phi_{-1}\right]$$

APPENDIX B: WALL FUNCTIONS

In this approach, the viscosity-affected inner region (viscous sublayer and buffer layer) is not resolved. Yet, some functions are used in order to link the solution variable at the first computational cell to the corresponding quantities on the wall. Basically, in our case, such functions have to include:

- Laws of the wall for mean velocity
- Formulas for near wall turbulent quantities.

These functions mainly rely on the work of Launder and Spalding [1974]. The way this work has been used in the Fluent code is the following:

The law of the wall for mean velocity (on the first computational node) yields:

$$\frac{U_p}{C_\mu^{1/4}k_p^{1/2}}=\frac{1}{\kappa}\ln\left[Ey_p\frac{(C_\mu^{1/2}k_p)^{1/2}}{\nu}\right]$$

In this last expression, U_p and y_p are, respectively, the time-average velocity of the fluid at the computational point P and the distance of the point P from the wall. E is an empirical constant (set to 9.0 but can depend on the roughness of the wall) and ν stands for the molecular viscosity of the fluid.

The diffusion of kinetic energy at the wall is set to zero:

$$\left.\frac{\partial k}{\partial n}\right|_w=0$$

This yields the value of the kinetic energy k_p at the computational point P.

Finally the dissipation is computed by using the following relation:

$$\varepsilon_p=\frac{C_\mu^{3/4}k_p^{3/2}}{\kappa y_p}$$

NOMENCLATURE

A	: area that allows the evaluation of the swirl number
C_μ	: constant as defined in Eq. (5)
d	: internal diameter of the primary injector
d_h	: hydraulic diameter of the annulus
d_0	: internal diameter of the annular device
D	: combustion chamber diameter
E	: averaged error as defined by Eq. (7)
k	: turbulence kinetic energy
l	: turbulence characteristic length scale
L	: combustion chamber length
N	: number of experimental data points
r	: radial spatial co-ordinate
$\bar{r}$	: average radius
S	: swirl number as defined in Eq. (10)
u_i	: instantaneous velocity
$\overline{u_i}$	: average velocity
u_i'	: velocity fluctuation
U	: axial component of the average velocity
U_a	: axial component of the maximum average velocity in the primary duct
U_{axe}	: axial component of the average velocity on the symmetry axis
U_s	: axial component of the average velocity in the secondary duct
U_0	: axial component of the average velocity on the symmetry axis at the inlet
V	: average velocity vector
W	: circumferential component of the average velocity
x	: axial spatial co-ordinate
y	: wall distance

Greek Letters

ε : rate of dissipation of the turbulence kinetic energy
ϕ_{exp} : experimental value of a physical quantity at a given point
ϕ_{num} : numerical value of a physical quantity at a given point
μ : molecular viscosity
μ_t : turbulent viscosity
ν : kinematics molecular viscosity
ρ : density

REFERENCES

Berat, C., "Contribution à la Mise au Point d'un Programme de Simulation Numérique d'un four à Charbon Pulvérisé," Thèse de l'Ecole Supérieure des Mines de Paris, Janvier (1987).

Boussinesq, J., "Théorie de l'écoulement Tourbillonnant," Mémoire Présenté par la Division Savante, Paris (1877).

Bradshaw, P., Launder, B. E. and Lumley, J. L., "Collaborative Testing of Turbulence Models," *Journal of Fluids Engineering*, **118**, 243, June (1996).

Brighton, J. A. and et Jones, J. B., "Fully Developed Turbulent Flow in Annuli," *Journal of Basic Engineering*, 835, December (1964).

Durao, D. and et Whitelaw, J. H., "Turbulent Mixing in the Developing Region of Coaxial Jets," *Journal of Fluids Engineering*, 467,473, September (1973).

Elena, L. and Schiestel, R., "Turbulence Modeling of Rotating Confined Flows," *International Journal of Heat and Fluid Flow*, **17**, 283, June (1996).

Fluent User's Guide, Version 4.4; Fluent : Lebanon, NH (1996).

Habib, M. A. and et Whitelaw, J. H., "Velocity Characteristics of Confined Coaxial Jets with and without Swirl," *Journal of Fluids Engineering*, **102**, 47 (1983).

Hogg, S. and Leschziner, M. A., "Computation of Highly Swirling Flow with a Reynolds Stress Turbulence Model," *American Institute of Aeronautics and Astronautics Journal*, **27**, 57, January (1989).

Hogg, S. and Leschziner, M. A., "Second Moment Closure Calculation of Strongly Swirling Confined Flow with Large Density Gradients," *International Journal of Heat and Fluid Flow*, **10**, 16, March (1989).

Launder, B. E. and Spalding, D. B., "Mathematical Models of Turbulence," Academic Press, London, England (1972).

Launder, B. E. and Spalding, D. B., "The Numerical Computation of Turbulent Flows," *Computer Methods in Applied Mechanics and Engineering*, **3**, 269 (1974).

Launder, B. E., Reece, G. J. and Rodi, W., "Progress in the Development of a Reynolds-Stress Turbulence Closure," *Journal of Fluid Mechanics*, **68**, 537, April (1975).

Launder, B. E., "Second Moment Closure: Present... and Future?," *International Journal of Heat and Fluid Flow*, **10**, 282 (1989).

Leschziner, M. A. and Rodi, W., "Calculation of Annular and Twin Parallel Jets Using Various Discretization Schemes and Turbulence-Model Variations," *Journal of Fluids Engineering*, **103**, 352, June (1981).

Lien, F. S. and Leschziner, M. A., "Upstream Monotonic Interploation for Scalar Transport with Application to Complex Turbulent Flows," *International Journal of Numerical Methods in Fluids*, **19**, 527 (1994).

Lien, F. S. and Leschziner, M. A., "Assessment of Turbulence Transport Models Including Non-Linear RNG Eddy Viscosity Formulation and Second-Moment Closure for Flow over a Backward-Facing Step," *Computers Fluids*, **23**, 983 (1994).

McKenty, F., Gravel, L. and Camarero, R., "Numerical Simulation of Industrial Boilers," *Korean J. Chem. Eng.*, **16**, 482 (1999).

Menter, F. R., "A Comparison of Some Recent Eddy-Viscosity Turbulence Models," *Journal of Fluids Engineering*, **118**, 514, September (1996).

Modaress, D., Wuerer, J. and Elgobashi, S., "An Experimental Study of a Turbulent Round Two-Phase Jet," American Iinstitute of Aeronautics and Astronautics/American Society of Mechanical Engineers - 3rd Joint Thermophysics, Fluids, Plasma and Heat Transfer Conference, Saint Louis, June (1982).

Monnot, G., "La Combustion dans les fours et les Chaudières," Publications de l'industrie française du pétrole (1978).

Ohtsuka, M., "Numerical Analysis of Swirling Non-Reacting and Reacting Flows by the Reynolds Stress Differential Method," *International Journal of Heat and Mass Transfer*, **38**, 331 (1995).

Patankar, S. V., "Numerical Heat Transfer and Fluid Flow," Hemisphere Publishing Corporation, Washington, DC (1980).

Rodi, W., "Turbulence Models and Their Application in Hydraulics," Delft, The Netherlands, I.A.H.R. (1984).

So, R. M. C., Ahmed, S. A. and Mongia, H. C., "An Experimental Investigation of Gas Jets in Confined Swirling Air Flow," NASA Contractor Report 3832, Sep. (1984).

Wilcox, D. C., "Turbulence Modeling for CFD," DCW Industries (1994).

Yakhot, V. and Orszag, A., "Renormalization Group Analysis of Turbulence. I. Basic Theory," *Journal of Scientific Computing*, **1**, 3 (1986).